

Regular Spectra and Universal Directionality of Emitted Radiation from a Quadrupolar Deformed Microcavity

Jeong-Bo Shim and Hai-Woong Lee*

Department of Physics, Korea Advanced Institute of Science and Technology, Daejeon, 305-701, Korea

Sang-Bum Lee, Juhee Yang, Songki Moon, Jai-Hyung Lee, and Kyungwon An
School of Physics, Seoul National University, Seoul, 151-742, Korea

Sang Wook Kim

Department of Physics Education, Pusan National University, Busan 609-735, Korea

(Dated: October 26, 2018)

We have investigated quasi-eigenmodes of a quadrupolar deformed microcavity by extensive numerical calculations. The spectral structure is found to be quite regular, which can be explained on the basis of the fact that the microcavity is an open system. The far-field emission directions of the modes show unexpected similarity irrespective of their distinct shapes in phase space. This universal directionality is ascribed to the influence from the geometry of the unstable manifolds in the corresponding ray dynamics.

I. INTRODUCTION

Symmetrical (cylindrical or spherical) microcavities have attracted much attention in the past as laser resonators, due to their compact and simple geometry, easiness to fabricate, and ultra-high Q values, which is attributed to formation of the so-called whispering gallery modes (WGM's) [1]. The isotropic radiation pattern of light emitted from the symmetrical microcavity, however, reduces their practical usefulness. One way to overcome this problem, as has been proposed by Nöckel et al., is to deform the shape to construct asymmetric resonant cavities (ARC's) [2, 3]. Directional emission has indeed been observed experimentally from asymmetrically deformed microlasers made of semiconductors [4, 5], dye jets [6] and polymers [7].

Fundamental optical properties of ARC's can be partly understood in terms of the ray dynamics. From the classical dynamical viewpoint, it belongs to a class of systems having mixed-type phase space, i.e., a mixture of both regular and irregular trajectories [8, 9, 10]. When deformation is very small, the phase space is dominated by regular rays of whispering gallery type and these rays escape from the cavity only by evanescent leakage (tunnelling). At larger deformations, however, emission properties are mainly determined by chaotic rays that diffuse stochastically and refract out of the resonator when the angle of incidence χ reaches the critical angle χ_c , i.e., $\sin \chi_c = 1/n$, where n is the refractive index of the resonator. This simple ray dynamics model predicts that at large deformations the escape occurs primarily into the tangential direction near the points of maximum curvature [2, 11].

Although the model captures the essence of the direc-

tional property of emitted radiation from ARC's, there may exist other complications. For example, a phenomenon referred to as dynamical eclipsing [12] occurs when stable islands occupy the phase space region at which the escape would have taken place without them, resulting in strong suppression of emission intensity in directions predicted by the ray model and appearance of split peaks in nearby directions. There are evidences that stable or unstable periodic orbits strongly influence the emission pattern of ARC. The emission originating from bow-tie modes [4, 13], whose corresponding classical orbit is a stable island, and the so-called scarred modes of hexagonal [6] and triangular [5] unstable periodic orbits, has been observed. So far the direction of the far-field emission obtained in experiments has been a commonly used tool to investigate the characteristics of the lasing mode of ARC, since it has been assumed that the shape of the wavefunction inside the cavity strongly influences or sometimes even completely governs the far-field emission pattern. It has been reported, however, that, due to the correction with Fresnel coefficients, the emission direction of the mode with a rather smaller Q value can be considerably deviated from an expectation based upon the above simple assumption [5]. Deviations from the prediction of the simple ray dynamics model also occur when the nonlinear effect of a medium is involved [14].

The simple ray dynamics model has recently been refined by Schwefel et al. [7]. They found that highly directional emission patterns from ARC's persist well beyond the deformation limit predicted from the ray model [2], and developed a more accurate model which emphasizes the importance of unstable manifolds of short periodic orbits. However, they did not show the direct evidence of the crucial role played by unstable manifolds in connection with their structure embedded in quantum wavefunctions. A similar analysis has been reported by Lee et al. in a stadium shaped microcavity, although the authors did not precisely mention the role of the unstable

*Electronic address: hwlee@laputa.kaist.ac.kr

manifolds [15].

The main purpose of this paper is to investigate optical properties of a quadrupolar micro-resonator with low refractive index ($n = 1.361$) by extensive numerical calculations. The reason why we choose the specific refractive index is that this work is initiated from our previous experiment of the dye-jet microcavity laser [6]. We would like to deliver two main results: firstly the energy level distribution shows deviations from an expectation from the usual random matrix theory (RMT), and secondly the far-field emission direction exhibits a nontrivial universal feature.

To a certain degree, optical properties of ARC's can be understood by using an analogy with chaotic dynamical properties of the billiard system which has been extensively studied in the context of nonlinear dynamics. The quantum mechanical manifestation of classical chaos, referred to as quantum chaos, has generally revealed that there is a close relation between the classical nonlinear dynamics (whether it is regular or chaotic) and quantum spectral statistics (whether the energy level spacing distribution is described by Poissonian or Wigner) [16]. Based on this observation, one might expect that there also exists close correlation between the ray dynamics and the statistical properties of the eigemodes of ARC's. Specifically, energy levels may be regularly distributed at small deformations, where the ray dynamics is predominantly regular, while they may look quite irregular at large deformations where chaotic rays dominate. We will show, however, that this simple expectation does not exactly hold true. There is an essential difference between ARC and the billiard system: The former is an open system while the latter is a closed one. The openness of ARC raises a nontrivial question: Where is the emitted output directed? This is completely meaningless in a closed system. Although the analogy between ARC and the billiard system is a useful starting point because the billiard has been thoroughly studied in the past, one cannot push the analogy too far.

This paper is organized in the following way: In Section II, we briefly explain both the ray dynamics and the wave properties of a quadrupolar billiard, and a quadrupolar deformed microcavity (QDM). In Section III, we show numerical results for spectra and far-field emission directionality of a QDM and discuss the regularity of the spectra and the universal directionality we obtained from the numerical computations. Finally in Section IV, we present a conclusion.

II. A QUADRUPOLEAR DEFORMED MICROCAVITY

When a liquid jet with circular cross section is deformed, its cross section can in general be described by

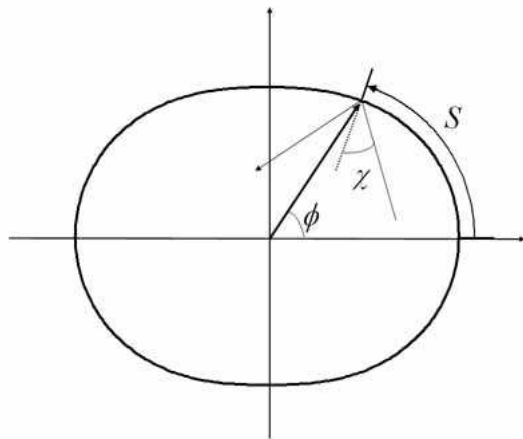


FIG. 1: A schematic view of Birkhoff coordinates: They consist of the distance along the boundary $S(\phi)$ and the reflection angle, χ . To make them canonically conjugate, $\sin \chi$ is used instead of χ .

the following multipole expansion [17]

$$r(\phi) = \frac{1}{2}a_0 + \sum_{j=1}^{\infty} a_j \cos j\phi + \sum_{j=1}^{\infty} b_j \sin j\phi, \quad (1)$$

where r is the distance from the center and ϕ the azimuthal angle. The lowest order even-symmetric quadrupolar contribution becomes dominant when the perturbation inducing deformation is small. The cross section of the dye jet can then be described by

$$r(\phi) = \frac{r_0}{\sqrt{1 + \varepsilon^2/2}} (1 + \varepsilon \cos 2\phi), \quad (2)$$

where r_0 and ε are respectively the radius of the undeformed (circular) cavity and the deformation parameter. The denominator in Eq. (2) guarantees that the cross sectional area is conserved irrespective of ε , which is consistent with the experimental condition of Ref. [6]. In this paper we focus on such a specific ARC, i.e., a QDM.

A. A quadrupolar billiard: closed system

At first, we consider the ray dynamics of a QDM with hard walls, namely a quadrupolar billiard. The Birkhoff coordinate system is quite useful to study the ray dynamics in a billiard. It consists of two variables S (or equivalently ϕ) and $\sin \chi$, which respectively represent the arc length of the position at which the ray strikes the boundary and the sine of the incident (or reflected) angle at the boundary [18] (Fig. 1). In Fig. 2 we show the Poincaré surfaces of section (PSOS) of the dynamics in the quadrupolar billiard by using Birkhoff coordinates. It exhibits a typical Kolmogorov-Arnold-Moser scenario [19], i.e. the evolution toward stochastic behavior as the deformation parameter ε is increased.

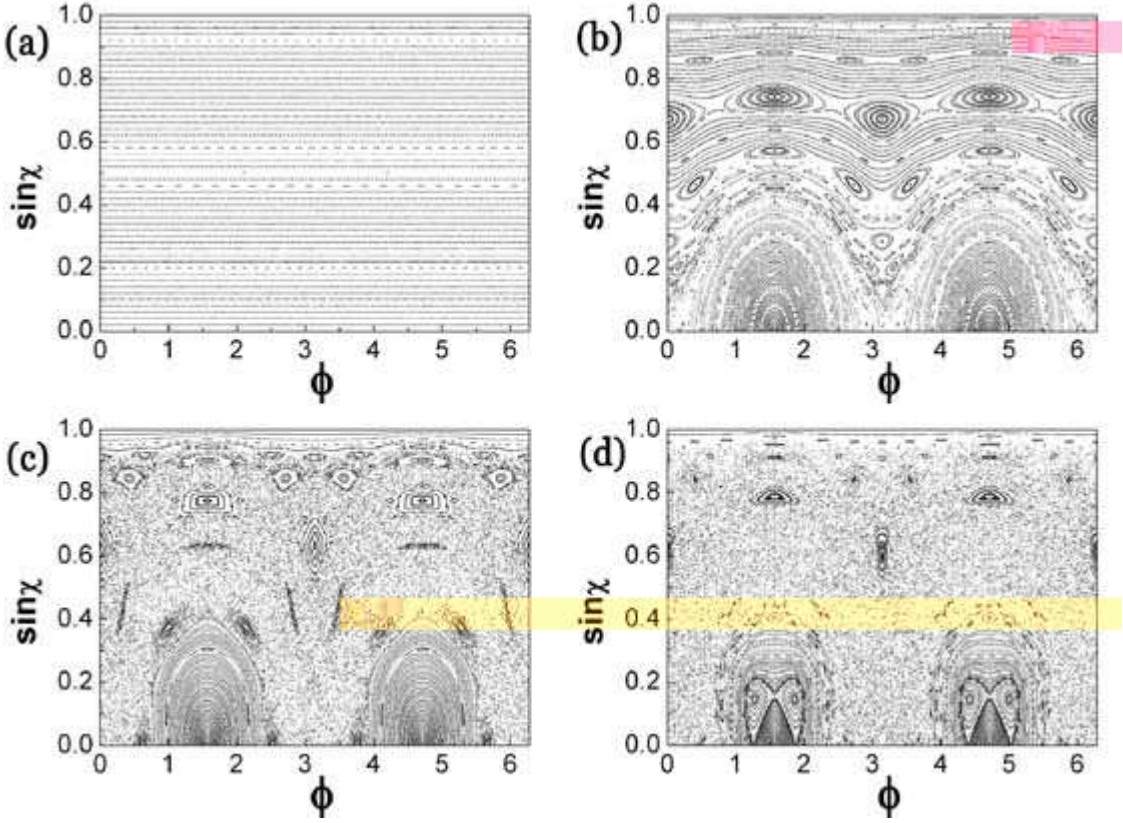


FIG. 2: The Poincaré surfaces of section of a quadrupolar billiard for (a) $\varepsilon = 0$, (b) $\varepsilon = 0.05$, (c) $\varepsilon = 0.10$, and (d) $\varepsilon = 0.12$.

The wave nature of a quadrupolar billiard can be described by the following Helmholtz equation with Dirichlet boundary condition

$$\nabla^2 \psi(r) + k^2 \psi(r) = 0, \quad (3)$$

where k is the wave number. For a circular billiard, the solution of Eq. 3 takes the form $J_m(r) \exp(im\phi)$, where J_m is a Bessel function. All the eigenvalues k_{lm} are analytically determined and form a well organized structure since they are just the l th zeros of the m th order Bessel functions. When a circular billiard is deformed, however, the distribution of eigenvalues starts to deviate from the regular structure. For large enough deformations, in which case the corresponding ray dynamics is predominantly chaotic, the well established RMT plays an important role. Although the nearest neighbor level spacing distribution of eigenvalues is described by the universal Wigner function, the eigenvalues themselves show quite a complex structure due to a lot of avoided crossings. Fig. 3 shows the evolution of eigenvalues (kr) as a function of the deformation parameter.

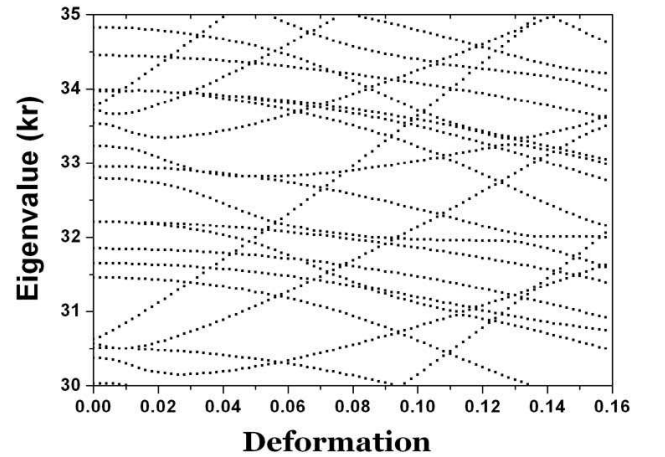


FIG. 3: Evolution of the eigenvalues as a function of ε . It shows a complicated structure.

B. A quadrupolar deformed microcavity: open system

A QDM is an open system in the sense that the ray with the incident angle larger than a critical angle is allowed to escape from the cavity. It does not make any

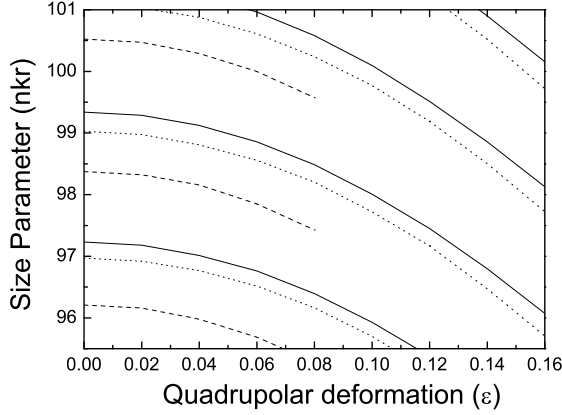


FIG. 4: Evolution of the real part of the eigenvalues of the mode with $l = 1$ (the dotted line), $l = 2$ (the solid line), and $l = 3$ (the dashed line) of a QDM as a function of ε .

influence on the ray dynamics itself inside the cavity, but reduces available phase space: e.g. for $n = 1.361$ the phase space area below $\sin \chi_c = 1/n \approx 0.73$ can be ignored.

The wave properties of an open system somewhat differ from those of a closed one. The eigenvalues of Eq. (3) now take complex values. Their imaginary part is associated with the decay rate of the mode. To quantify the decay rate, a cavity quality factor Q defined as $-2 \times k_r / k_i$, where k_r and k_i are respectively real and imaginary parts of the eigenvalue, is commonly used. The real part of the eigenvalue is represented by the size parameter defined as $nk_r r_0$, which is abbreviated as nkr if there is no confusion.

As far as a circular microcavity is concerned, Eq. (3) is still separable so that two good quantum numbers, radial (l) and angular ones (m), can be well defined. The eigenvalues k_{lm} are analytically given by matching between Bessel and Neumann functions. Similarly to a circular billiard, one can see the well-defined free spectral range (FSR) among the modes with the identical radial quantum number l .

Figure 4 presents a continuous variation of the real part of eigenvalues as the deformation is increased. Surprisingly, the eigenvalues vary quite regularly in comparison with the complicated structures in Fig. 3. This regular structure remains, although the deformation becomes large enough to generate global chaos in classical dynamics. The monotonic decrease of nkr implies the red shift of spectral lines. In case of WGM it can be explained by considering an elongated optical path due to deformation. In order to explain the regularity of spectrum, we need to investigate more carefully the nature of the modes. In the following section their phase space distribution will be discussed based mainly upon the Husimi plot.

When the system is open, a question naturally arises: Into which direction is the output field emitted? In a circular cavity, the emission direction should be isotropic due to the circular symmetry, while it is highly non-trivial to address it for ARC's. In the viewpoint of the ray dynamics, the emission direction is determined from the position $(\phi, \sin \chi)$ at which the incident angle of the ray becomes equal to the critical angle. In wave mechanics, however, one should find quasi-eigenmodes, which are an open system analogue to eigenmodes of a closed system, by direct numerical calculation. In this work we use the boundary element method to compute quasi-eigenmodes [20, 21].

III. REGULAR SPECTRUM AND UNIVERSAL EMISSION DIRECTIONALITY

In this section we discuss the origin of the regularity of the spectrum and the universal emission directionality. The Husimi distribution function is a very powerful tool to study these issues.

A. The Husimi plot of the eigenmode of the deformed microcavity

The Husimi distribution function can be regarded as a mathematical description of the phase-space distribution in which the minimum-uncertainty Gaussian wave packet is used as a basis [22]:

$$H_\psi(q_0, k_0) = \left| \int \psi(q) \xi(q - q_0, k_0) dq \right|^2, \quad (4)$$

where

$$\xi(q - q_0, k_0) = \exp \left[-\frac{(q - q_0)^2}{2\sigma} + ik_0(q - q_0) \right]. \quad (5)$$

In order to obtain the Husimi plot in Birkhoff coordinates, it is necessary to modify Eqs. (4) and (5). Taking it into account that ϕ is 2π periodic, the basis function ξ can be rewritten as

$$\xi(\phi - \phi_0, \sin \chi) = \sum_l \exp \left[-\frac{(\phi + 2\pi l - \phi_0)^2}{2\sigma} + ik \sin \chi (\phi - \phi_0) \right], \quad (6)$$

and the integration in Eq. (4) should be taken from 0 to 2π [23, 24]. For our calculation we set the width of the gaussian as $\sigma = \sqrt{2}/k_0$.

In Fig. 5 we present Husimi plots of several quasi-eigenmodes obtained numerically. The $l = 1$ modes in a circular cavity evolves from a horizontally flat shape to the distribution localized somewhere in the phase space in Fig. 5(c). A similar evolution is also observed in the $l = 2$ modes except that it is localized on the period-6

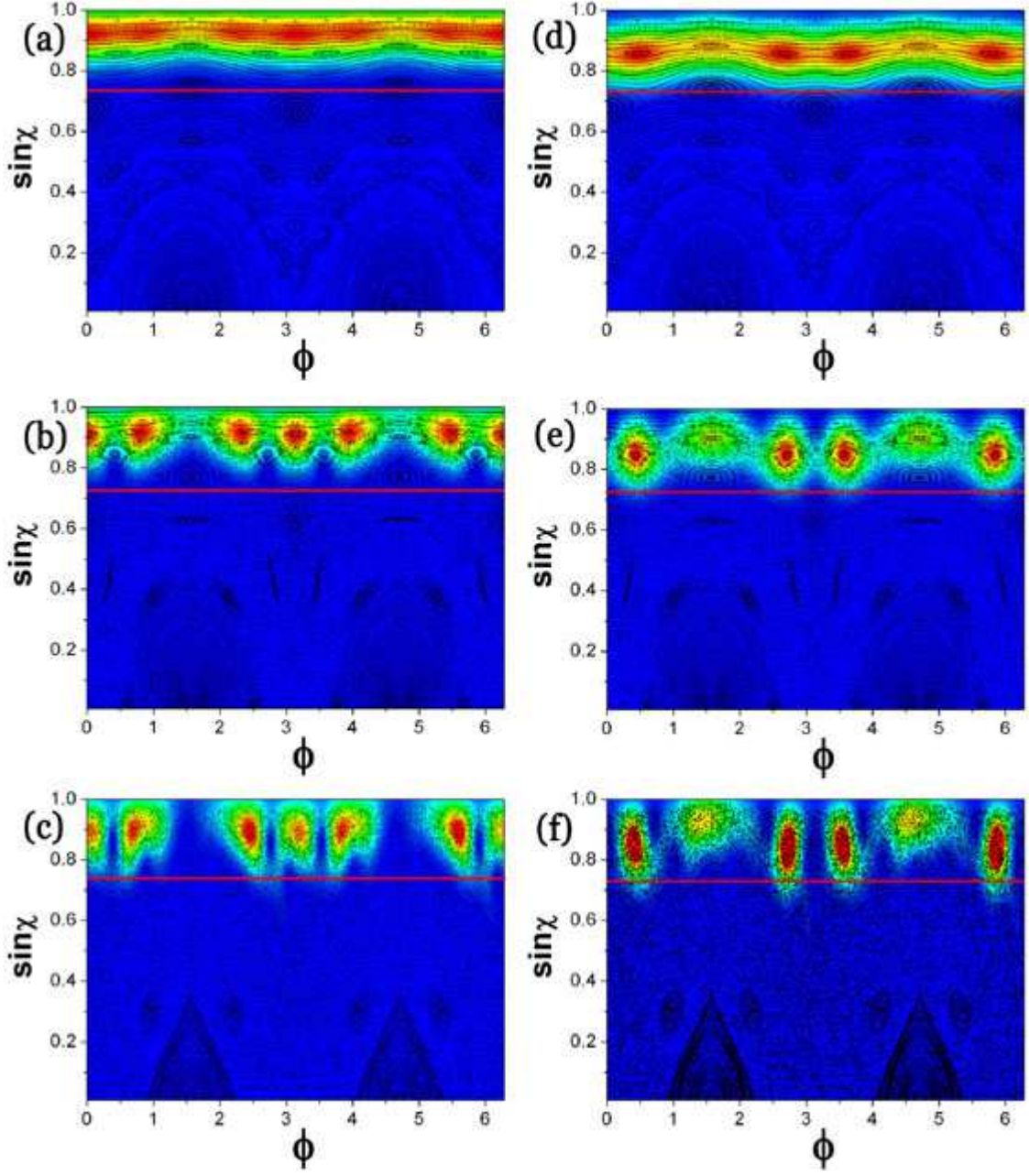


FIG. 5: Husimi plots of a QDM with (a) $\varepsilon = 0.05$, (b) 0.1 and (c) 0.16 for the $l = 1$ modes, and with (d) $\varepsilon = 0.05$, (d) 0.1 and (f) 0.16 for the $l = 2$ modes. The corresponding complex size parameters are (a) $96.64 - i0.003$, (b) $96.89 - i0.004$, (c) $95.87 - i0.004$, (d) $96.10 - i0.005$, (e) $96.25 - i0.014$, and (f) $96.61 - i0.029$. The critical line defined by $\sin\chi_c = 1/n$ is indicated with the red horizontal lines.

orbit which loses its stability around $\varepsilon \sim 0.12$. The $l = 2$ modes then forms a hexagonal shaped scarred mode extensively investigated in our previous work [6]. All the modes identified with $l = 2$ in Fig. 4 appear to have the similar shapes in Husimi plots as shown in Fig. 6. It is more difficult to identify the corresponding classical orbit of the $l = 1$ modes. It seems to correspond to the period-6 orbit based upon Fig. 5(c), since it has six enhanced localized probability maxima in the phase space.

However, their locations along the vertical axis ($\sin\chi$) fit themselves to those of the period-8 orbit. Interestingly, this mode exactly corresponds to the period-8 orbit for larger nkr . We believe that the $l = 1$ mode is experiencing the transition from the period-6 to the period-8 orbit. More details will be discussed elsewhere.

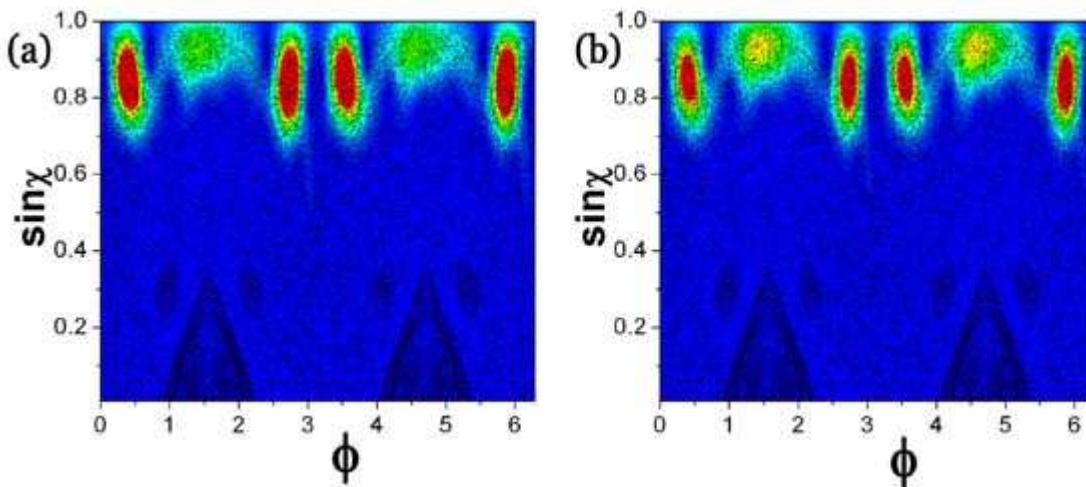


FIG. 6: Husimi plots of the $l = 2$ mode at (a) $nkr = 96.073$ and (b) $nkr = 98.12$ for $\varepsilon = 0.16$. These two modes are separated by two units of FSR.

B. Regular spectra

In closed systems, chaotic states which are irregularly distributed over available phase space are frequently observed, so that they strongly interact with and repel each other to generate avoided crossings and form complicated spectral structures as shown in Fig. 3. In contrast, quasi-eigenmodes in open systems hardly form chaotic states. The reason is that the chaotic modes have too small Q values to form modes in the practical sense, since they decay in a short time due to refractive escape. In Fig. 4 the $l = 3$ mode seems to disappear at $\varepsilon \sim 0.08$, which implies that it is difficult to find the mode due to a very small Q , since, for a given nkr , the larger l is the smaller Q is. The mode with even larger l (> 3) may exist in Fig. 3 but is practically meaningless, because Q is extremely low. One may more frequently find chaotic modes for larger nkr , because Q is exponentially enhanced as nkr is increased. It leads us to the conclusion that in open systems chaotic quasi-eigenmodes are rarely observed unless nkr is large enough.

It is no wonder that non-chaotic modes show deviations from the prediction based upon RMT, since they are localized somewhere in phase space. It is unlikely that for a given nkr the $l = 1$ mode has a similar shape with the $l = 2$ mode. In the semiclassical theory [25] the larger l the bigger the incident angle of the ray. It implies that the modes with different l 's form distinct shapes in phase space. It is clearly shown in Figs. 5(c) and (f) that those two modes hardly overlap with each other. As ε is increased, they independently evolve with their own shape maintained in phase space. That explains the regular spectral structure observed in Fig. 4.

C. Universal emission directionality

The quasi-eigenmodes of an open system contain evanescent waves outside the cavity, which cause decay of the modes in time. Figures 7(a) and (b) show that some of the waves leak out, which cannot be seen in the Husimi plot. The output directionality is in practice the most important characteristics that we seek from ARC's. It is more definitely illustrated by the far-field emission intensity as a function of the output direction as shown in Figs. 7(c) and (d). Surprisingly, these two figures demonstrate an almost identical pattern whose maximum is located around 40° . It should be emphasized that the corresponding Husimi plots of these two modes differ from each other as shown in Figs. 5(c) and (f). Since it has been believed that the emission direction is determined from the internal shape of the quasi-eigenmode, it is necessary to explain this unexpected observation.

The clue for the origin of the identical far-field directionality irrespective of the shapes of a quasi-eigenmode comes out of the fact that the far-field pattern obtained from ray dynamics shown in Fig. 8(d) is not much different from those from the wave calculations. In the ray calculations, the ray incident with the angle smaller than the critical angle is reflected in or emitted out with the probability determined by Fresnel coefficients.

In a long time the ray dynamics in the chaotic region is governed by the so-called unstable manifolds [19]. They are easily seen by launching a set of localized initial conditions of rays in quadrupolar billiard and following the dynamics for a few tens of collisions [see Figs. 8(a) and (b)]. As time goes to the infinity, the ray dynamics in a closed system will finally become ergodic so that the rays are uniformly distributed over phase space. As far as an open system is concerned, however, rays escape from a cavity before reaching uniform distribution. Therefore, the available phase space is limited, and the dynamics in

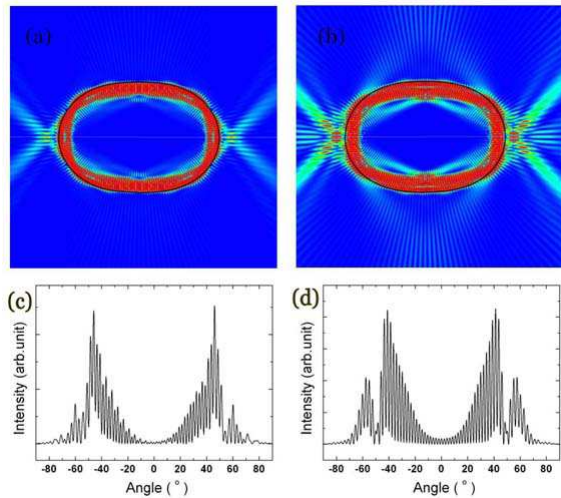


FIG. 7: Probability distributions of the wavefunctions of the quasi-eigenmodes in real space for (a) $nkr = 97.72$ ($l = 1$) and (b) $nkr = 98.12$ ($l = 2$). The far-field emission intensities are shown for (c) the mode corresponding to (a) and (d) the mode corresponding to (b).

the restricted space is described by the motion along a few dominant unstable manifolds. As a result, the unstable manifolds dominate the long (but not extremely long) time dynamics in ARC's, and consequently the output directionality. In Fig. 8(c), we plot the accumulated intensity in phase space, obtained by recording the Birkhoff coordinates at which each ray escapes and totaling the number of the escaped rays weighted by Fresnel refractive coefficients at each phase space point $(\phi, \sin\chi)$. The intensity pattern resembles the structure of the unstable manifolds shown in Fig. 8(b). In Fig. 8(d) we show the far field emission intensity obtained from the ray dynamics calculations, which is seen to be consistent with the results of the wave calculations shown in Figs. 7(c) and 7(d).

The unstable manifolds can also be found through a careful examination of Husimi plots, as Figs. 9(a) and 9(b) indicate. Such a fine structure could not be seen in the original Husimi plots of Figs. 5, because it is associated with a tiny probability. No matter how small the probability associated with the unstable manifold is, it significantly overlaps the region below the critical angle. It means that this fine structure mainly contributes to the output directionality regardless of the tiny probability, unless the Q value is not too small. Note that $Q \sim 10^4$ for both the $l = 1$ and $l = 2$ modes. We may now conclude that, based on both the ray dynamics calculations and the wave calculations, the emission di-

rectionality is determined mainly by the structure of the unstable manifolds.

In order to show that the above conclusion is quite general, we also investigate the Husimi plots and the far-field emission directionality of the modes for larger nkr , namely ~ 200 . Figures 10 (a)-(e) show a variety of shapes of Husimi plots of the modes: For example, (b) is an octagonal and (d) is a hexagonal scarred mode. Another interesting point found in Fig. (10) is that each mode does not have any considerable overlap with the others. In this sense, every mode in Fig. 10 is quite distinct from one another. Surprisingly again, the far-field emission directions are almost identical for all such five *distinct* modes as shown in Fig. 11. As mentioned above, it is also attributed to the geometry of the unstable manifolds as clearly seen in Figs. 10(f)-(j). Therefore, we call the identical far-field emission directionality determined from the unstable manifolds a *universal* directionality.

IV. CONCLUSION

In this work we have studied spectral properties and mode structure of a quadrupolarly deformed microcavity and the output directionality of the radiation emitted from it. We summarize the main conclusion of our work.

(1) When the system is open like a QDM, chaotic orbits no longer easily form a quasieigenmode since their Q values are expected to be very low due to the refractive escape. Consequently the localized modes such as scarred ones are more frequently observed in comparison with the usual closed chaotic system. This explains the regular structure of the spectrum with well-defined level spacings even at large deformations.

(2) The direction of the radiation emitted from a quadrupolar microcavity resonator is determined mainly by the geometry of the unstable manifolds of the resonator. As the geometry of the unstable manifolds is governed by classical dynamical properties of the resonator and thus is independent of the structure of the excited modes, the output directionality exhibits universality, largely independent of the degree of deformation and the pump power.

Acknowledgments

This work was supported by the KOSEF Grant (R01-2005-000-10678-0). JBS and HWL were supported by a grant from KRISS. SNU group is supported by the KOSEF Grants(NRL-2005-01371). SWK was supported by the KRF Grant (KRF-2004-005-C00044).

[1] Y. Yamamoto and R. E. Slusher, *Physics Today* **46**, 66 (1993).

[2] J. Nöckel and A. D. Stone, *Nature* **385**, 45 (1997).

[3] A. D. Stone, *Physica A* **288**, 130 (2000).

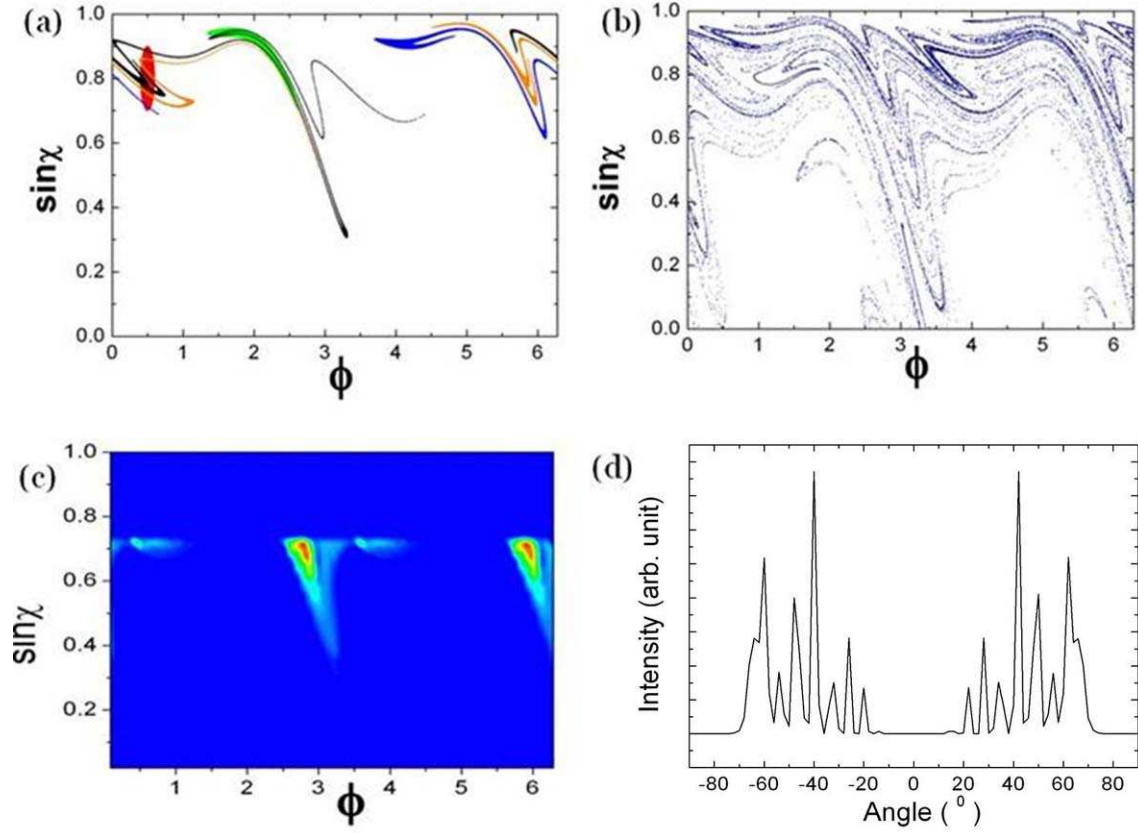


FIG. 8: Time evolution of the rays starting from a set of 10^4 initial conditions localized on the upper left side of the phase space and far-field emission intensity. (a) The rays after a few steps. (b) The rays after 20 collisions on the boundary (the complicated structure of unstable manifold manifest themselves). (c) The accumulated intensity of the escaped rays weighted by Fresnel refractive coefficients. (d) The far-field emission intensity obtained from the ray dynamics.

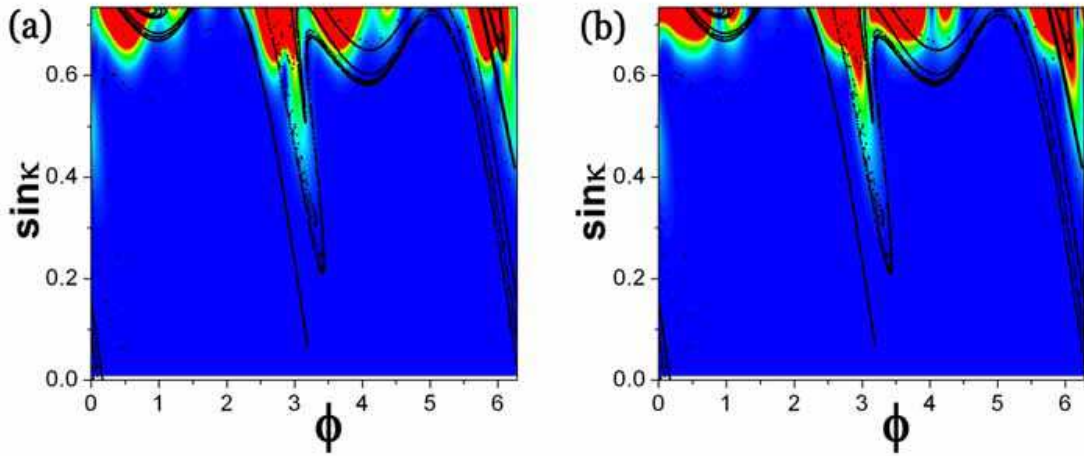


FIG. 9: An expanded view of the Husimi plots of (a) Fig. 5(c) and (b) Fig. 5(f) for the region below the critical angle. The unstable manifolds are shown in the background with black curves.

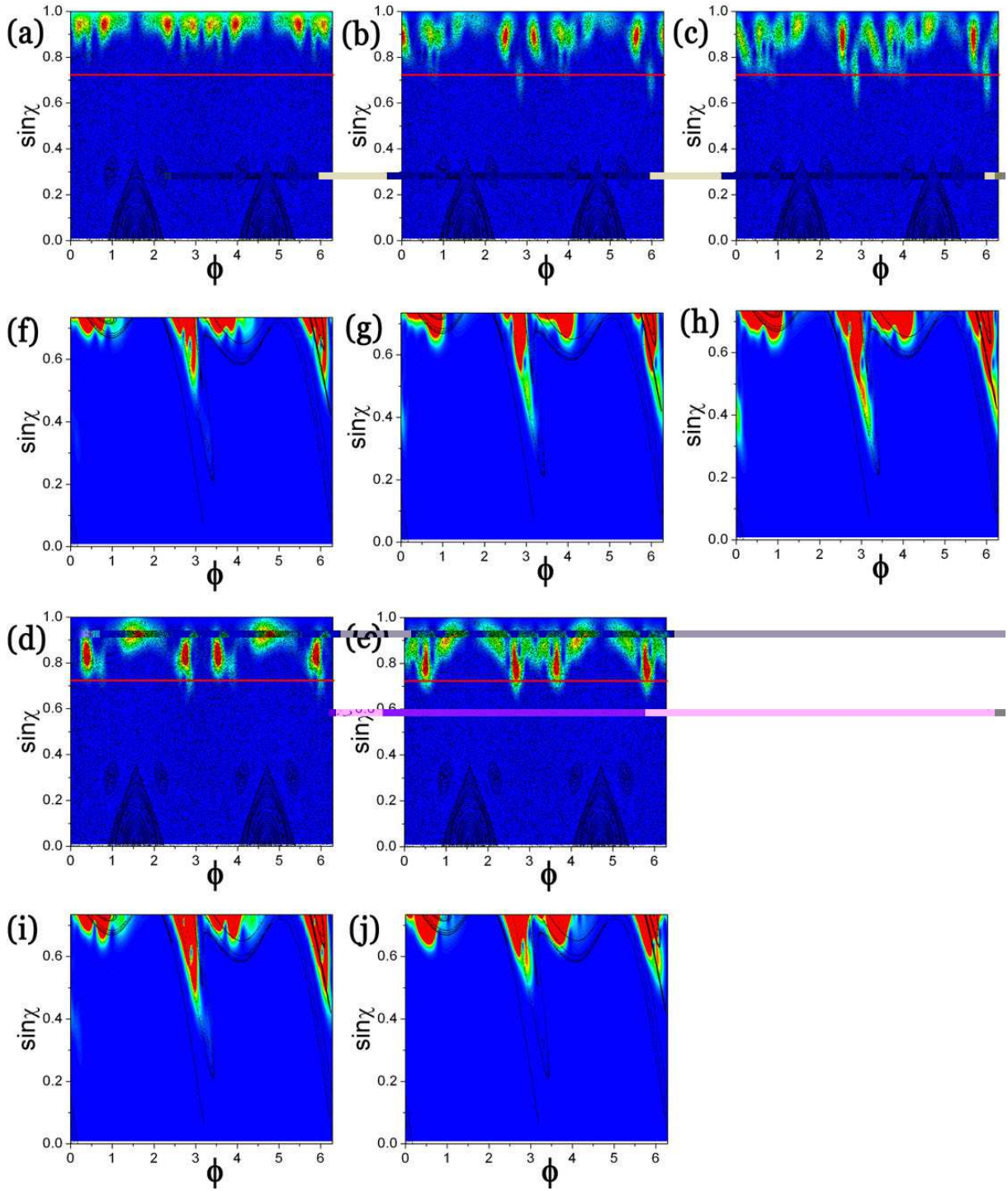


FIG. 10: Husimi plots of various modes for $\varepsilon = 0.16$ whose complex size parameters are respectively (a) $228.87 - i0.002$ ($l = 1$), (b) $232.27 - i0.018$ ($l = 2$), (c) $226.30 - i0.027$ ($l = 3$), (d) $227.65 - i0.018$ ($l = 4$), and (e) $230.86 - i0.021$ ($l = 5$). (f)-(j) expanded views of the Husimi plots of (a)-(f) for the region below the critical angle. The critical line defined by $\sin\chi_c = 1/n$ is indicated with the red horizontal lines on (a)-(e). The unstable manifolds are shown in the background with black curves on (f)-(j).

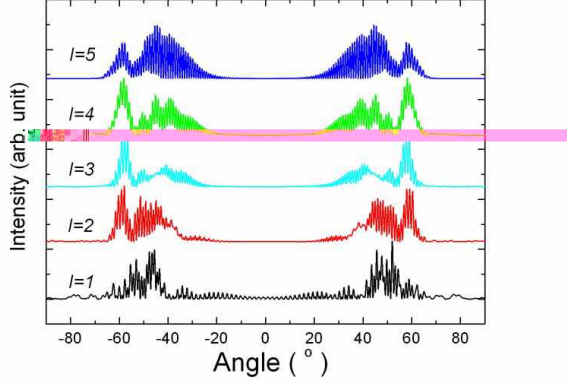


FIG. 11: The far-field emission distributions associated with the five modes presented in Fig. 10.

- [4] C. Gmachl, F. Capasso, E. E. Narimanov, J. Nöckel, A. D. Stone, J. Faist, D. Sivco, and A. Cho, *Science* **280**, 1556 (1998).
- [5] N. B. Rex, H. E. Tureci, H. G. L. Schwefel, R. K. Chang, and A. D. Stone, *Phys. Rev. Lett.* **88**, 094102 (2002).
- [6] S.-B. Lee, J.-H. Lee, J.-S. Chang, H.-J. Moon, S. W. Kim, and K. An, *Phys. Rev. Lett.* **88**, 033903 (2002).
- [7] H. G. L. Schwefel, N. B. Rex, H. E. Tureci, R. K. Chang, A. D. Stone, T. ben Massoud, and J. Zyss, *J. Opt. Soc. Am. B* **21**, 923 (2004).
- [8] S. W. Kim and H. W. Lee, *Phys. Rev. E* **59**, 5384 (1998).
- [9] I. C. Percival, *Journal of Physics B* **6**, L229 (1973).
- [10] O. Bohigas, S. Tomsovic, and D. Ullmo, *Physics Report* **223**, 43 (1993).
- [11] J. Nöckel, A. D. Stone, and R.K.Chang, *Optics Letter* **19**, 1693 (1994).
- [12] S. S. Chang, J. Nöckel, R. K. Chang, and A. D. stone, *JOSA B* **17**, 1828 (2000).
- [13] J. Nöckel, A. D. Stone, and R.K.Chang, *Optics Express* **10**, 752 (2002).
- [14] P. D. Takehisa Harayama and K. S. Ikeda, *Phys. Rev. Lett.* **82**, 3803 (1999).
- [15] S.-Y. Lee, J.-W. Ryu, T.-Y. Kwon, S. Rim, and C.-M. Kim, *Phys. Rev. A* **72**, 061801 (2005).
- [16] F. Haake, *Quantum Signatures of Chaos* (Springer-Verlag, 1991).
- [17] H. Lamb, *Hydrodynamics* (Dover, New York, 1945).
- [18] G. D. Birkhoff, *Acta. Math* **50**, 359 (1927).
- [19] Lichtenberg and Lieberman, *Regular and Stochastic Motion* (Springer-Verlag New York Inc., 1983).
- [20] S. Kagami and I. Fukai, *IEEE Trans. Antennas Propag.* **32**, 455 (1984).
- [21] J. Wiersig, *Journal of Optics A* **5**, 53 (2003).
- [22] H.-W. Lee, *Physics Report* **259**, 147 (1995).
- [23] G. P. B. Crespi and S.-J. Chang, *Phys. Rev. E* **47**, 986 (1993).
- [24] M. Hentschel and H. Schomerus, *Europhys. Lett.* **62**, 636 (2003).
- [25] J. Nöckel, Ph.D. thesis, Yale University (1997).